International Journal of Computational and Experimental Science and ENgineering (IJCESEN)

Vol. 10-No.1 (2024) pp. 15-20
http://www.ijcesen.com

ISSN: 2149-9144

Research Article

The Optical Properties of Galaxy Cluster Abell 2319

Ebru AKTEKİN ÇALIŞKAN*

Süleyman Demirel Üniversity, Science and Arts Faculty, Physics Department, 32200, Isparta-Türkiye
* **Corresponding Author** : **Email:** ebrucaliskan@sdu.edu.tr - **ORCID:** 0000-0002-5904-4580

Article Info:

DOI: 10.22399/ijcesen.236
Received : 12 November 2023
Accepted : 08 December 2023

Keywords
galaxies: clustering
galaxies: structure
techniques: photometric
techniques: spectroscopic

Abstract:

The optical photometric and spectroscopic investigations of the massive and merging galaxy cluster Abell 2319 (A2319) are presented here. RTT150 telescope of TÜBİTAK, Antalya, Türkiye used CCD imaging and spectroscopic observations. In this paper, 110 galaxies were determined in A2319 and defined as the magnitudes of the Bessel B and R filters in each cluster member galaxy. Spectral observations were done of the brightest cluster galaxy (BCG) and six additional brilliant galaxies. We estimated the Luminosity Function (LF) of galaxies for each filter. The resulting LF of cluster galaxies for each filter is well-fitted by the Double Schechter function. The best-fit parameter values derived as the characteristic absolute magnitudes are -21.08 ± 0.03, and -20.84 ± 0.01, -21.43 ± 0.02, and -20.54 ± 0.02, and the slopes at the faint end of the LF were -1.34 ± 0.04 and -1.12 ± 0.03, -1.47 ± 0.05 and -1.18 ± 0.03 for B and R filters, respectively.

1. Introduction

Galaxy clusters are the universe's largest known structures and are made up of more than 50 galaxies, hot ionized gas in hydrostatic balance that fills the inner cluster environment, and dark matter. Because of their size and dynamic structure, they are the structures that best depict the universe. Detailed optical wavelength analyses of galaxy clusters allow for the analysis of galaxy content and distribution in the clusters [1, 2, 3]. The Luminosity function (LF) provides the number of galaxies in a given volume that have a specified luminosity. Galaxies' LFs are a valuable tool for testing theories of galaxy formation and evolution [4]. The first study on LF was conducted by [5, 6]. Schechter [5, 6] provided a mathematical equation for LF that is consistent with the findings in this investigation. Bond et al. [7] revitalized and expanded on Schechter [5][6] function and theory. The following is the Schechter function:

$$\emptyset(M)d(M) = \emptyset^{*}10^{0.4(M^{*}-M)(1+\alpha)}\exp\left[-10^{0.4(M^{*}-M)}\right]dM \qquad (1)$$

Here, ϕ (M) d(M) the number density of galaxies with dM, ϕ^{*} is the normalization, α is the faint-end slope and M^{*} is the characteristic absolute magnitude.

Faint galaxy mergers in clusters affect LFs in galaxies. These effects are investigated using LFs. Some galaxy clusters have LF dips and increases [8]. In galaxies optical spectra, emission line intensity ratios can differentiate between various nebular gas ionization mechanisms, including shocks, AGN, and H II regions [9, 10]. Whereas [OIII] is dependent on the ionization parameter and gas-phase metallicity, Hβ is mainly influenced by ionizing radiation. The diagnostic lines that trace the characteristics of gas in star-forming regions are the recombination line Hβ and the optical emission line doublet [OIII] λλ4959, 5007 Å. Whereas [O III] is dependent on the ionization parameter and gas phase metallicity, Hβ is mainly influenced by ionizing radiation.

These two diagnostics, together with additional lines, can be used to assess the hardness, ionization parameter, metallicity, and electron temperature of the radiation field in the interstellar medium (ISM) of a star-forming galaxy [11]. In the Baldwin–Phillips Terlevich (BPT) diagram [9], [O III]/Hβ is used in conjunction with [N II]/Hα to discriminate between galaxies powered by active galactic nuclei (AGNs) that inhabit a specific region of BPT parameter space characterized by elevated emission line ratios, and starforming galaxies that lie along the H II abundance sequence. The metallicity, ionizing radiation field, and ISM conditions of star-forming galaxies determine their precise location on the HII sequence [12].

A2319 has been extensively studied in the optical, radio, and X-ray bands in the past decades. Optical analyses of the bright galaxies in A2319 [e.g., 13, 14, 15] suggested that it consists of two separate components superimposed along the line of sight: a sub-cluster around the second brightest galaxy, at about 10 northwest (NW) of the main concentration. The brightest cluster galaxy (BCG), is CGCG 230-007. Dynamical studies in the optical band [see e.g. 14 and references therein] have shown that the cluster is composed of two main clumps: the main cluster and a sub-cluster localized some 10 arcmin; northwest of the cD galaxy and behind the main cluster. At radio wavelengths, A2319 is permeated by a radio halo [16], approximately oriented in the northeast-southwest direction. Asymmetric X-ray emission and a powerful cluster-scale radio halo indicate that A2319 is a merging cluster of galaxies [17]. The fundamental physical properties of A2319 are given in Table 1.

Table 1. *General properties of A2319.*

Parameters	Value	References
Classified	BM type II-III	[18]
Richness	1	[19]
Type	RS-type cD	[20]
RA(J2000)	$19^h\ 20^m\ 45^s.30$	[21]
Dec(J2000)	$43^0\ 57'\ 43''$	[21]
Redshift	0.0559	[22]

Here, we present a thorough examination of optical CCD imaging and spectroscopic data related to the massive nearby cluster A2319 (z = 0.0559). Section 2 provides a description of the optical observations and data reduction. In Section 3, we present our results and discussion, while our main conclusions are given in Section 4.

2. Material and Methods

2.1. Optical Imaging Data Analysis

The observations are performed with the Russian Turkish 1.5-m Telescope (RTT150). The seeing conditions were consistent throughout the whole observations within a range of 1.8 arcsec. The RTT150 has a Ritchey-Chretien optical system functioning together with Cassegrain and Coude focal systems. We used a TUG Faint Object Spectrograph and Camera (TFOSC), with the f/7.7 focal ratio Cassegrain low-resolution faint object spectrograph and camera throughout our observations. In our imaging observations, we used a CCD camera consisting of 2048 × 2048 pixels, each measuring 15 μm × 15 μm, covering a 13 × 13 arcmin field of view (FoV). Because of its angular size, A2319 was divided into 16 regions, and each region was inspected separately. Our imaging observations were completed by using Bessel B and R band filters. The log of imaging observations is given in Table 2.

Table 2. *Log of Imaging Observations*

Date	Exposure (s)	Filter	FWHM (nm)	λ_{cent} (nm)
2015 Sep 11	300x3	Bessel V	100	519
2015 Sep 12	300x3	Bessel R	128	600

An Image Reduction and Analysis Facility (IRAF) was used to process the raw data and reduce it. Standard procedures were used for data reduction, including bias corrections, over-scan at the field, and cosmic ray exclusion using the IRAF CCDPROC package. The positions of red stars from the USNO A2.0 catalogue Monet et al. [23] were used to examine the source's locations. The instrumental magnitudes of all cluster member galaxies were determined using the Point Spread Function (PSF) method. Our photometry is calibrated to the VEGA-MAG system. The mosaic image was created by combining optical images from 16 different images. Figure 1 presents optical mosaic image of A2319 in Bessel R filter.

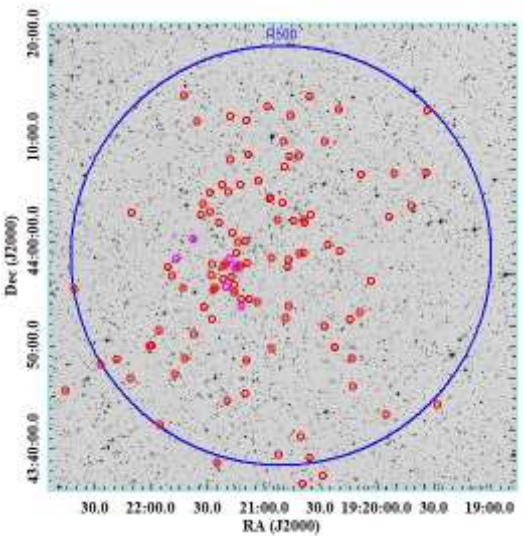

Figure 1. *Integrated (total) optical RTT150 image of A2319 in the Bessel R filter. The brightest member of the cluster CGCG+07-40-004 and six galaxies whose spectra were taken are shown with circles. All other galaxies that are members of the cluster are shown with red circles in the figure.*

For cluster member galaxies, LFs were obtained in the B and R filters. As a function of the absolute B and R magnitudes, the resulting LFs were computed in bins of 0.5 mags. The LFs obtained in this investigation did not suit a single Schechter function well. This is characterized by a dip or plateau about -22.53 mag for B and -22.47 mag for R, followed by an increase. As a result, a double Schechter function represents both LFs. They are shown in Figure 2.

Table 3 includes the best-fit Schechter parameter as well as the χ^2.

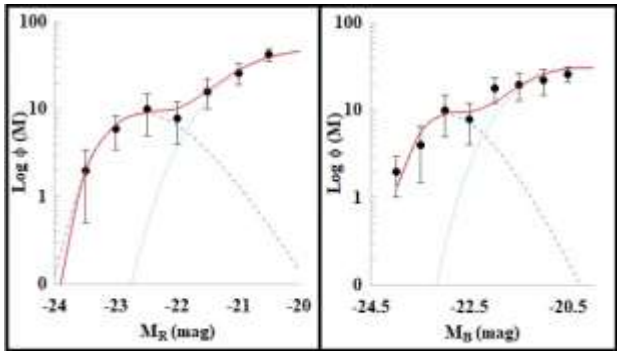

Figure 2. *LF of A2319 in the R (left) and B (right) bands. The Double Schechter function is shown by a continuous red line. The blue dashed line and blue continuous line depict the individual components of the double Schechter fit.*

Table 3. *The best-fit parameters of Luminosity Function for A2319 in the B and R Bands*

Filter	M*	**α**	χ^2
B	-21.8±0.03 -20.84±0.01	-1.34±0.04 -1.12±0.03	0.78
R	-21.43±0.02 -20.54±0.02	-1.47±0.05 -1.18±0.03	0.82

2.2. Optical Spectral Data Analysis

On August 12, 2015, we conducted our spectrum measurements using the RTT150 Cassegrain-TFOSC/CCD. Using the grism G15, spectral data were obtained in the λ3230-9120 Å range. Using a notional dispersion of about 8 Å pixel^{-1}, the grism G15 was employed. A total of seven distinct regions' spectra have been examined. The slit width we used during our spectral observations was 1.78 arcsec (100 μm). The Longslit context package of IRAF is used for spectrum reduction and analysis. The exposure time for each spectrums is 900 s. For the flux calibration, we have observed the standard star (HR 8634) as our spectrophotometric standard as suggested by [24, 25]. For every observation, Fe-Ar calibration lamp frames with a slit width of 100 microns were acquired. The spectrum of CGCG 230-007 is given in Figure 3 and the spectra of the other 6 point galaxies are given in Figure 4 in the λ 4000-7000 Å range. We list the flux with 1 σ errors, BCG and the 6 point-like sources (galaxies) spectrum emission lines, their fluxes and 1σ error for the observed spectral lines in Table 4.

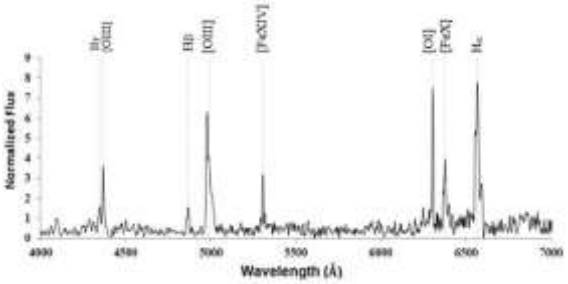

Figure 3. CGCG 230-007 *(BCG of the cluster) spectrum in the range of λ 4000-7000 Å. Its Balmer Hα λ6563 Å, Hβ λ4861 Å, Hγ λ4341 Å , forbidden lines [OIII] λ 4363, 5007 Å , [FeXIV] λ5303 Å , [OI] λ6300 Å, [FeX] λ6374 Å and [NII] λ λ 6548, 6584 Å are shown.*

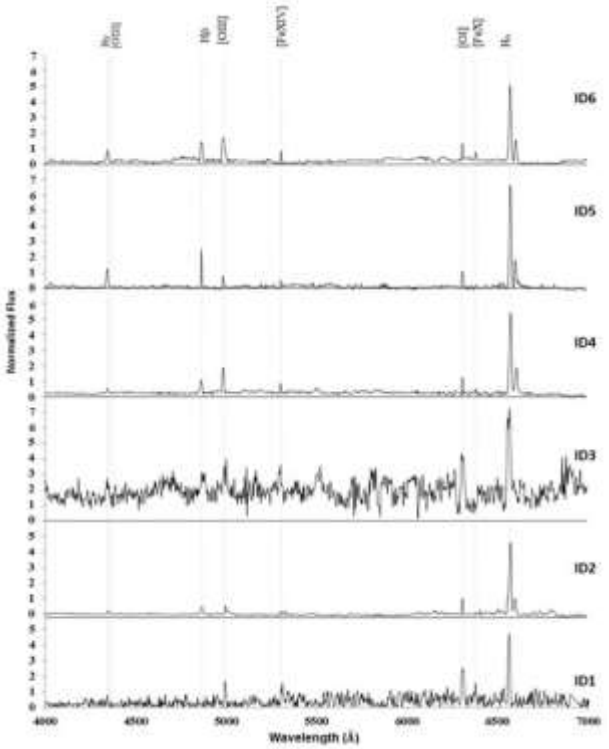

Figure 4. *Spectra of 6 point sources (galaxies) in λ 4000-7000 Å range. Their Hα λ6563 Å, Hβ λ4861 Å, Hγ λ4341 Å, forbidden lines [OIII] λ 5007 Å , and [NII] λ λ 6548, 6584 Å are shown.*

3. Results and Discussions

We report on our spectroscopic and optical imaging observations of a nearby galaxy cluster with a previously detected radio halo that roughly follows the X-ray-emitting gas A2319.

3.1. Imaging

We used the Bessel B and R filters in optical imaging.

Table 4. *BCG (CGCG 230-007) and the 6 point-like sources (galaxies) spectrum emission lines and their fluxes with 1 σ errors.*

	Flux x 10^{-17} (erg s^{-1} cm^{-2})						
Lines (Å)	**BCG**	**ID1**	**ID2**	**ID3**	**ID4**	**ID5**	**ID6**
Hγ λ 4340	16.41±2.32	2.75±1.32	1.15±0.02	8.81±3.73	2.80±0.03	6.36±0.08	4.64±0.09
[OIII] λ4363	36.13±2.30	-	-	-	-	-	-
Hβ λ 4861	17.98±2.40	-	2.7±0.01	9.53±3.74	5.56±0.04	12.51±0.07	7.33±0.11
[OIII] λ 5007	61.50±2.24	8.41±1.37	2.57±0.01	15.05±3.73	9.38±0.05	4.01±0.07	8.67±0.10
[FeXIV] λ 5303	30.71±2.35	-	-	-	-	-	-
[OI] λ 6300	74.68±2.44	-	-	-	-	-	-
[FeX] λ 6374	41.82±2.45	-	-	-	-	-	-
[NII] λ 6584	49.67±2.52	-	-	-	-	-	-
Hα λ 6563	78.33±2.30	23.75±1.33	23.02±0.03	31.14±3.12	27.11±0.04	33.42±0.06	25.43±0.08
[NII] λ 6584	30.53±2.45	-	4.98±0.02	6.83±4.72	9.28±0.03	8.97±0.07	7.88±0.09

The optical images obtained for each filter were used for determining the magnitude, and redshifts were utilized to calculate the absolute magnitudes. Figure 2 shows LFs, which are the absolute magnitude distributions of galaxies in the B and R filters, independently for each filter. In LFs, there is a large decrease followed by a rise in the B filter at M = -22.53 magnitude and M = -22.47 magnitude in the R filter. It seems that the observed cluster's richness influences how much LF decreases.

LFs are not well represented by a single monotonic Schechter function but show a 'dip' or 'plateau' at intermediate luminosities, followed by a power-law rise at lower luminosities. According to Phillipps & Driver [26] and Popesso et al. [27], these might be best-fit by a double Schechter function or a single Schechter function with a power law. This demonstrated that LF exhibited bimodal behaviour and that a two-component function was better appropriate for defining it. As a result, the distribution was expressed using the double Schechter function. For each filter, the most appropriate parameters of the double Schechter function, which was determined as a two-mode function, were found. The chi-square indicates that the Double Schechter is a better fit to the LF. The $\chi 2$ values, which indicate a likelihood of less than 0.90, were considered acceptable. The method was repeated until the best 2 was produced, resulting in the best Double Schechter parameters. The typical absolute magnitudes of -21.08 ± 0.03, -20.84 ± 0.01, -21.43 ± 0.02, and -20.54 ± 0.02, are the best-fit parameter values that were calculated. The filters with B and R had slopes at the faint end of the LF of -1.34 ± 0.04 and -1.12 ± 0.03, -1.47 ± 0.05, and -1.18 ± 0.03, respectively.

3.2. Spectroscopic

We obtained spectra of BCG and six galaxies in A2319. The BCG showed Balmer Hα λ6563 Å, Hβ λ4861 Å, Hγ λ4341 Å and forbidden emission lines ([OIII] λ λ 4363, 5007 Å, [FeXIV] λ 5303 Å, [OI] λ 6300 Å, [FeX] λ 6374 Å, and [NII] λ λ 6548, 6584 Å) in its spectrum. The remaining six galaxies are Hα λ6563 Å, Hβ λ4861 Å, Hg λ4341 Å, as well as the forbidden lines [OIII] λ 5007 Å and [NII] λλ 6548, 6584 Å.

Some of the most luminous AGN kinds are Seyfert 1. Their non-stellar continuum and strong, broad permitted emission lines make them identifiable. Our obtained spectra imply that Seyfert 1 is one of these seven galaxies. The peculiar emission lines and spectra of these galaxies point to a galaxy of the Seyfert 1 type. [OIII]5007/Hβ ≥ 3 is the secondary classification criterion [28]. This ratio is 3.59 for BCG.

The optical spectrum also shows rather strong 'coronal' lines such as [FeX] λ6375 and [FeXIV] λ 5303. We show that these lines could come from the warm absorber's outer regions, but stronger collision strength calculations for these transitions are needed to resolve this issue completely.

4. Conclusions

- **i.** The LFs in both filters showed a significant decline, then a rise. Therefore, A2319 can be considered a Rich galaxy cluster.
- **ii.** The best-fit parameters for LFs for both filters as determined by Double Schechter: -21.08 ± 0.03, -20.84 ± 0.01, -21.43 ± 0.02, and -20.54 ± 0.02.
- **iii.** Using Double Schechter, the tide end slopes for both filters were determined to be -1.34 ± 0.04 and -1.12 ± 0.03, -1.47 ± 0.05 and -1.18 ± 0.03.
- **iv.** The unique emission lines and matching ratios detected in all seven spectra demonstrate Seyfert 1 galaxies.

Author Statements:

- **Ethical approval:** The conducted research is not related to either human or animal use.
- **Conflict of interest:** The authors declare that they have no known competing financial interests or personal relationships that could have appeared to influence the work reported in this paper

- **Acknowledgement:** We appreciate the valuable comments given by the referee and we thank TÜBİTAK-TUG for their support in using RTT150 (Russian-Turkish Telescope) for our observations performed through Project number 15BRTT150-869.
- **Author contributions:** The authors declare that they have equal right on this paper.
- Funding information: The authors declare that there is no funding to be acknowledged
- **Data availability statement:** The data that support the findings of this study are available on request from the corresponding author. The data are not publicly available due to privacy or ethical restrictions.

References

[1]. Turner, D. J., Giles, P., Romer, A. K., Wilkinson, R. D., Upsdell, E. W., Klein, M., Viana, P. T. P., Hilton, M., Bhargava, S., Collins, C., Mann, R., Sahlén, M., & Stott, J. P. (2022). The*XMM*Cluster Survey: an independent demonstration of the fidelity of the eFEDS galaxy cluster data products and implications for future studies. *Monthly Notices of the Royal Astronomical Society*, *517*(1), 657–674. https://doi.org/10.1093/mnras/stac2463

[2]. Erdim, M. K., Ezer, C., Unver, O., Hazar, F. A., & Hüdaverdi, M. (2021). The relative supernovae contribution to the chemical enrichment history of Abell 1837. *Monthly Notices of the Royal Astronomical Society*, *508*(3), 3337–3344. https://doi.org/10.1093/mnras/stab2730

[3]. McCleary, J., Dell'Antonio, I., & Von Der Linden, A. (2020). Dark Matter Distribution of Four Low-z Clusters of Galaxies. *The Astrophysical Journal*, *893*(1), 8. https://doi.org/10.3847/1538-4357/ab7c58

[4]. Feng, L., Yan, P., & Yuan, Q. (2014). Luminosity Function of The Galaxy Cluster Abell 85. *Chinese Astronomy and Astrophysics*, *38*(3), 247–256. https://doi.org/10.1016/j.chinastron.2014.07.003

[5]. Schechter, P. L. (1976a). An analytic expression for the luminosity function for galaxies. *The Astrophysical Journal*, *203*, 297. https://doi.org/10.1086/154079

[6]. Schechter, P. L. (1976b). An analytic expression for the luminosity function for galaxies. *The Astrophysical Journal*, *203*, 297. https://doi.org/10.1086/154079

[7]. Bond, J. R., Cole, S., Efstathiou, G., & Kaiser, N. (1991). Excursion set mass functions for hierarchical Gaussian fluctuations. *The Astrophysical Journal*, *379*, 440. https://doi.org/10.1086/170520

[8]. Durret, F., Adami, C., Cappi, A., Maurogordato, S., Márquez, I., Ilbert, O., Coupon, J., Arnouts, S., Benoist, C., Blaizot, J., Edorh, T. M., Garilli, B., Guennou, L., Brun, V. L., Fèvre, O. L., Mazure, A., McCracken, H. J., Mellier, Y., Mezrag, C., . . . Ulmer, M. P. (2011). Galaxy cluster searches based on photometric redshifts in the four CFHTLS Wide fields. *Astronomy and Astrophysics*, *535*, A65. https://doi.org/10.1051/0004-6361/201116985

[9]. Baldwin, J. A., Phillips, M. M., & Terlevich, E. (1981). Classification parameters for the emission-line spectra of extragalactic objects. *Publications of the Astronomical Society of the Pacific*, *93*, 5. https://doi.org/10.1086/130766

[10]. Dopita, M. A., & Sutherland, R. S. (2004). *Astrophysics of the diffuse universe*. Springer Science & Business Media.

[11]. Osterbrock, D. E. (1989). *Astrophysics of gaseous nebulae and active galactic nuclei*. Astrophysics of Gaseous Nebulae and Active Galactic Nuclei, by Donald E. Osterbrock. Published by University Science Books, ISBN 0-935702-22-9, 408pp, 1989.

[12]. Kewley, L. J., Groves, B., Kauffmann, G., & Heckman, T. M. (2006). The host galaxies and classification of active galactic nuclei. *Monthly Notices of the Royal Astronomical Society*, *372*(3), 961–976. https://doi.org/10.1111/j.1365-2966.2006.10859.x

[13]. Faber, S. M., & Dressler, A. (1977). Radial velocities for galaxies in 11 clusters. *The Astronomical Journal*, *82*, 187. https://doi.org/10.1086/112028

[14]. Oegerle, W. R., Hill, J. M., & Fitchett, M. J. (1995). Observations of high dispersion clusters of galaxies: constraints on cold dark matter. *The Astronomical Journal*, *110*, 32. https://doi.org/10.1086/117495

[15]. Trevese, D., Cirimele, G., & De Simone, M. (2000). An X- Ray and optical study of matter distribution in the galaxy cluster A2319. *The Astrophysical Journal*, *530*(2), 680–687. https://doi.org/10.1086/308381

[16]. Feretti, L., Giovannini, G., & Böhringer, H. (1997). The radio and X-ray properties of Abell 2319. *New Astronomy*, *2*(6), 501–515. https://doi.org/10.1016/s1384-1076(97)00034-1

[17]. Yan, P., Yuan, Q., Zhang, L., & Zhou, X. (2014). Multıcolor Photometry Of The Mergıng Galaxy Cluster A2319: Dynamıcs And Star Formatıon Properties. *The Astronomical Journal*, *147*(5), 106. https://doi.org/10.1088/0004-6256/147/5/106

[18]. Bautz, L. P., & Morgan, W. W. (1970). On the Classification of the Forms of Clusters of Galaxies. *The Astrophysical Journal*, *162*, L149. https://doi.org/10.1086/180643

[19]. Abell, G. O., Corwin, H. G., & Olowin, R. P. (1989). A catalog of rich clusters of galaxies. *Astrophysical Journal Supplement Series*, *70*, 1. https://doi.org/10.1086/191333

[20]. Struble, M. F., & Rood, H. J. (1982). Morphological classification /revised RS/ of Abell clusters in D less than or equal to 4 and an analysis of observed correlations. *The Astronomical Journal*, *87*, 7. https://doi.org/10.1086/113081

[21]. Mahdavi, A., & Geller, M. J. (2001). The LX-Σ relation for galaxies and clusters of galaxies. *The Astrophysical Journal*, *554*(2), L129–L132. https://doi.org/10.1086/321710

[22]. Wu, X., Fang, L., & Xu, W. (1998). Updating the σ-T relationship for galaxy clusters. *arXiv (Cornell University)*. https://doi.org/10.48550/arxiv.astro-ph/9808181

[23]. Monet, D., Canzian, B., Harris, H., Reid, N. H., Rhodes, A. B., & Sell, S. (1998). VIZIER Online Data Catalog: The PMM USNO-A1.0 Catalogue (Monet 1997). *yCat*. https://ui.adsabs.harvard.edu/abs/1998yCat.1243. ..0M/abstract

[24]. Hamuy, M., Suntzeff, N. B., Heathcote, S., Walker, A. R., Gigoux, P., & Phillips, M. M. (1994). Southern spectrophotometric standards, 2. *Publications of the Astronomical Society of the Pacific*, *106*, 566. https://doi.org/10.1086/133417

[25]. Hamuy, M., Walker, A. R., Suntzeff, N. B., Gigoux, P., Heathcote, S., & Phillips, M. M. (1992). Southern spectrophotometric standards. *Publications of the Astronomical Society of the Pacific*, *104*, 533. https://doi.org/10.1086/133028

[26]. Phillipps, S., & Driver, S. P. (1995). Are disappearing dwarfs just lying low? *Monthly Notices of the Royal Astronomical Society*. https://doi.org/10.1093/mnras/274.3.832

[27]. Popesso, P., & Biviano, A. (2006). The AGN fraction–velocity dispersion relation in clusters of galaxies. *Astronomy and Astrophysics*, *460*(2), L23–L26. https://doi.org/10.1051/0004-6361:20066269

[28]. Veilleux, S., & Osterbrock, D.E., (1987), Spectral Classification of Emission-Line Galaxies. *Astrophysical Journal Supplement , 63*, 295-310. https://doi.org/10.1086/191166